Montogue

Quiz FM112

Microfluidics

Lucas Monteiro Nogueira

PROBLEMS

Problem 1

Considering the elementary theory of microfluidics and electrokinetic flow, true or false?

Consider a potassium ion (K^+) in a water reservoir immersed in an electric field of intensity 12 kV/m. The measured electrophoretic mobility is $\mu_{EP} = 5.0\times10^{-8}$ m^2/(V·s) and the ion mass is $m = 6.5\times10^{-26}$ kg.

1.( ) The acceleration of the ion, assumed constant, can be calculated to be greater than 5×10^{10} m/s^2.

2.( ) The terminal velocity of the ion can be calculated to be greater than 500 µm/s.

3.( ) Consider a microchannel with cross-sectional area equal to 200 µm^2 and surface electroosmotic mobility equal to 1.6×10^{-8} m^2/V·s. If an electric field of 120 V/cm is applied to this microchannel, we may conclude that the resulting volumetric flow rate will be greater than 40,000 µm^3/s.

4.( ) Consider electroosmotic flow in a circular tube of diameter 8 µm and length 10 cm filled with an aqueous solution (viscosity $\mu = 10^{-3}$ Pa·s, relative permittivity $\varepsilon = 80$). For a potential $\zeta = -120$ mV, we surmise that a pressure drop of 0.8 atmospheres would suffice to generate at least the same total flow that would be generated by the application of a voltage of 1.5 kilovolts to this system.

5.( ) In order to characterize microfluidic channel cross-sections, some engineers have proposed use of the so-called *compactness factor*, a parameter usually defined as the ratio of a section's squared perimeter to its area. The compactness factor is also known as the *correction factor*, and the two terms can be used interchangeably.

In contrast to the case of planar diffuse double layers, the equations for diffuse double layers near curved surfaces are difficult to solve. When a spherical surface is considered, the corresponding Poison-Boltzmann equation in spherical coordinates for a $(z:z)$ electrolyte solution is written as

$$\frac{1}{r^2}\frac{d}{dr}\left(r^2\frac{d\psi}{dr}\right)=\frac{2ezn_\infty}{\varepsilon}\sinh\left(\frac{ze\psi}{k_bT}\right)$$

The Poisson-Boltzmann equation as written above assumes that ψ varies in the radial direction only. The typical boundary conditions are

$$\begin{cases}\psi=\psi_s \text{ at } r=a\\ \psi\to 0 \text{ at } r\to\infty\end{cases}$$

as illustrated to the side.

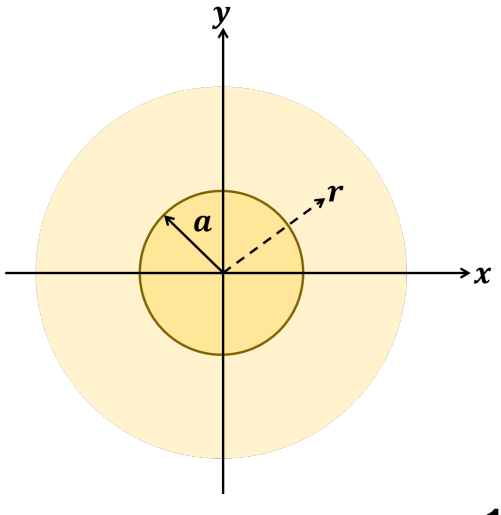

6.( ) Crucially, the Poisson-Boltzmann equation, when stated in spherical coordinates with the two boundary conditions specified above, has no analytical solution. ■ **(A black square indicates the end of a multi-paragraph statement.)**

7.( ) When a capillary tube is plunged into a volume of wetting liquid, the liquid rises inside the tube under the effect of capillary forces. Per the so-called *Jurin's law*, the height reached by the liquid is directly proportional to the radius of the tube.

8.( ) For microflows of small capillary number, it can be shown that the difference between dynamic and static contact angles is linearly related to the capillary number.

9.( ) A student in a microfluidics class was copying lecture notes for Taylor-Aris dispersion, but his S.O.B. professor cleared the blackboard before he could finish writing them down. As a result, the student ended up with the following incomplete PDE on his notebook. Knowing that the theory they were discussing pertains to circular microchannels. we can help him out and fill the blank rectangle with the number 210.

$$\frac{\partial \tilde{C}}{\partial t} = D\left(1 + \frac{\mathrm{Pe}^2}{\square}\right)\frac{\partial^2 \tilde{C}}{\partial z^2}$$

▶ Problem 2

Problem 2.1: Compute the Debye length of an electrical double-layer for a 10^{-3} M KCl solution at 298 K. The dielectric constant of KCl may be taken as 40. Use $\varepsilon_0 = 8.85\times10^{-12}$ C^2/N·m^2 as the vacuum permittivity, $e = 1.60\times10^{-19}$ C as the elementary charge, $k_B = 1.38\times10^{-23}$ J/K as Boltzmann's constant, and $N_A = 6.02\times10^{23}$ as Avogadro's number.

Problem 2.2: Show that the Debye length for an asymmetrical electrolyte in water at 298 K can be estimated as

$$k^{-1} = 4.30\times10^{-10}\left(\sum_i z_i^2 M_i\right)^{-1/2}$$

where z_i and M_i are the valence and molarity of the i-th ion, respectively.

Problem 2.3: Suppose that 800 mL of 0.02 M potassium chloride solution is mixed with 600 mL of 0.0018 M potassium sulfate. Using the formula derived in the previous part, find the Debye length for the resulting solution.

▶ Problem 3

Consider fully-developed laminar flow of an infinitely diluted (i.e., pure water, $n_\infty = 6.02\times10^{20}$ m^{-3}) aqueous 1:1 electrolyte solution through a slit microchannel. The separation distance is $a = 25$ μm and the channel is $L = 1$ cm long. The channel is under the effect of a zeta potential $\zeta = -100$ mV. At a temperature of 310 K, the physical and electrical properties of the liquid are electrical permittivity $\varepsilon = 88$, and dynamic viscosity $\mu = 9.0\times10^{-4}$ Pa·s. A pressure difference of 1 atm and an arbitrary chosen reference velocity $V_0 = 1$ m/s are considered. Plot the dimensionless velocity profile for this system, which is given by

$$\bar{V}_z = \frac{G_1}{2}\left(1-\bar{X}^2\right) - \frac{2G_2\bar{E}_s\bar{\zeta}}{K}\left[1 - \frac{\sinh\left(K\bar{X}\right)}{\sinh\left(K\right)}\right]$$

In this equation, $\bar{V}_z$ is the normalized axial velocity, $\bar{X} = x/a$ is the normalized distance between plates, and $\bar{E}_s = E_s/\zeta_0$ is the ratio of the applied electric field E_s to the zeta potential ζ_0 at the wall. Further, parameters G_1, G_2 and K are given in the Additional Information section.

▶ Problem 4

Consider thermal micro-Couette gas flow with viscous heating in the slip regime, $0.01 < Kn < 0.1$. Derive the adjusted velocity and temperature profiles.

▶ Problem 5

Problem 5.1: An often-used approximation for the flow rate Q induced by a pressure drop Δp on a rectangular microchannel is

$$Q \approx \frac{h^3 w \Delta p}{12 \mu L}\left(1 - 0.63\frac{h}{w}\right)$$

where h is the height of the section, w is the width, Δp is the pressure drop, μ is the viscosity of the fluid, and L is the length of the conduit. This expression is a simplified version of the exact solution

$$Q \approx \frac{h^3 w \Delta p}{12 \mu L}\left[1 - \sum_{n=1.3.5,\ldots}^{\infty} \frac{1}{n^5}\frac{192}{\pi^5}\frac{h}{w}\tanh\left(n\pi\frac{w}{2h}\right)\right]$$

Dividing Q from either the approximate or exact solution by Δp yields the inverse hydraulic resistance $R = Q/\Delta p$. Calculate the deviation in results implied by using the approximate equation instead of the exact one for a square section (i.e., such that $h = w$).

Problem 5.2: Show by paying special attention to the $n = 1$ term in the series Eq. (3.57*d*) that an improved approximation for reciprocal hydraulic resistance is

$$1/R \approx \frac{h^3 w}{12 \mu L}\left\{1 - \left[0.630 - \frac{192}{\pi^5}\left(1 - \tanh\left(\frac{\pi w}{2h}\right)\right)\right]\frac{h}{w}\right\}$$

and calculate for a square the deviation from the exact result.

▶ Problem 6

Consider a flat and very wide rectangular channel inside of which we have a liquid/gas interface. It is easy to show that, if the contact angle θ is the same for the top and bottom plates, the pressure drop can be easily estimated with the Young-Laplace equation

$$\Delta p = \frac{2\gamma}{h}\cos(\theta)$$

where γ is the interfacial surface tension and h is the height of the channel. Suppose now that the configuration is such that the contact angles for the top and bottom plate have values θ_1 and θ_2, respectively, with $\theta_1 \neq \theta_2$. Which of the following equations best approximates the pressure drop in this modified configuration?

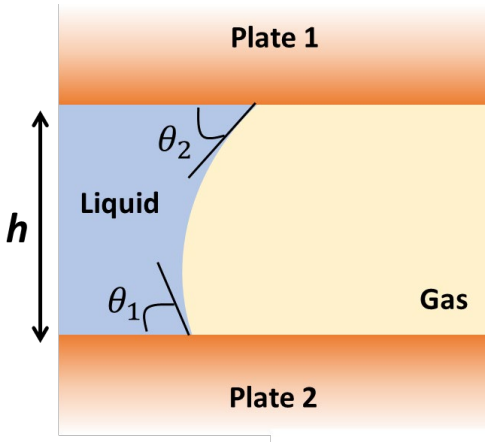

A) $\Delta p = \frac{2\gamma}{h}\cos\left(\frac{\theta_1 + \theta_2}{2}\right)$

B) $\Delta p = \frac{2\gamma}{h}\cos\left(\frac{|\theta_1 - \theta_2|}{2}\right)$

C) $\Delta p = \frac{2\gamma}{h}\left[\frac{\cos(\theta_1) + \cos(\theta_2)}{2}\right]$

D) $\Delta p = \frac{2\gamma}{h}\left[\frac{|\cos(\theta_1) - \cos(\theta_2)|}{2}\right]$

▶ Problem 7

Of particular interest in microfluid mechanics applications is the time required for a liquid column/meniscus to advance in a long horizontal microchannel of cross-sectional area $A = hw$, where h is channel height and w is channel width. Given fluid surface tension γ, dynamic viscosity μ, and contact angle θ, find an expression for the velocity of the advancing meniscus and the extent travelled $L(t)$.

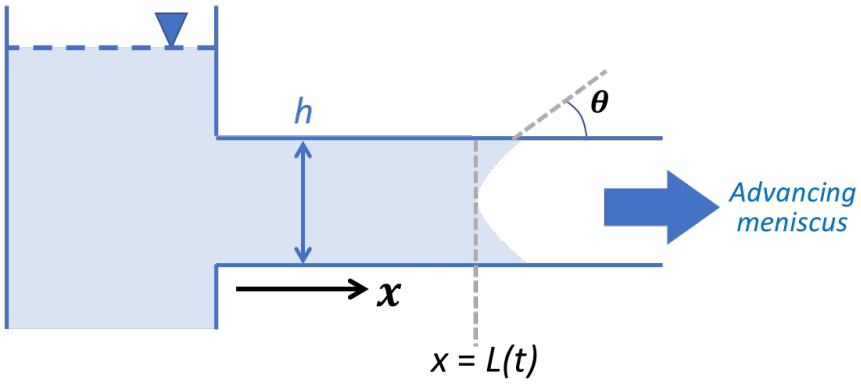

▶ Problem 8

Regarding advanced aspects of microfluidics and electroosmotic flow, true or false?

1.( ) Electroosmotic flow differs from conventional laminar flow in that the driving force is not a pressure gradient but an externally applied electric field. For comparison, one can establish the 'effective pressure' required to produce the same electroosmotic flow rate as in a conventional Poiseuille flow. The following figure shows the equivalent pressure gradient, in MPa/m, required to achieve the same microchannel osmotic flow (MCOF) at a certain electric field intensity, in kV/cm, for a circular microchannel. With reference to this graph, we see that, in order to sustain a MCOF at Reynolds number equal to 3, the effective pressure gradient required is greater than 10 MPa/m.

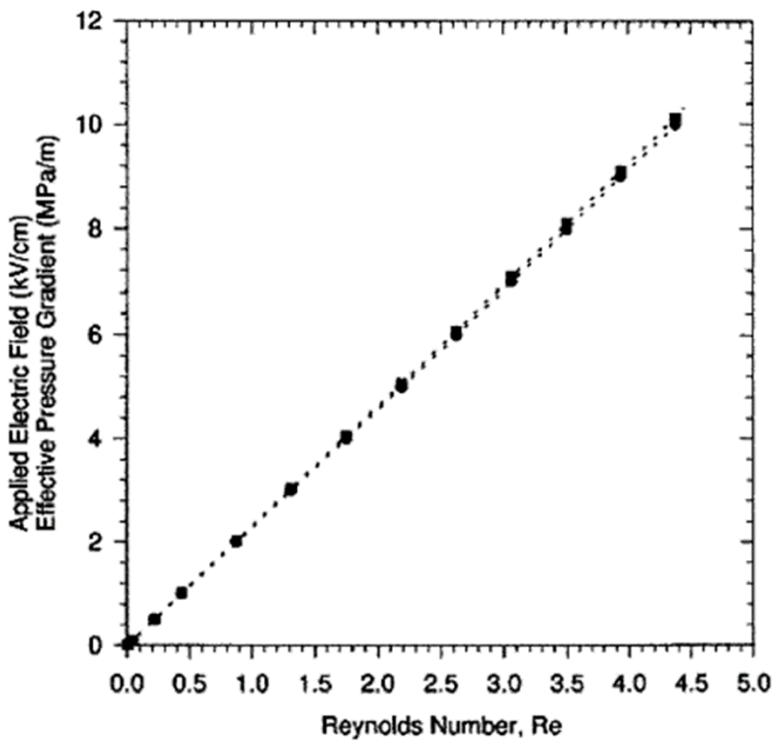

2.( ) Yang *et al.* (2001) used a finite difference code to analyze entrance effects for electroosmotic flow in a microchannel. The figure to the side shows a comparison of the entry lengths for an electroosmotic flow and for a typical pressure-driven flow at the same flow rate. From the figure, it can be gleaned that entrance lengths are generally greater for electroosmotic flow than for an equivalent pressure-driven flow.

Recommended research: Yang *et al.* (2001).

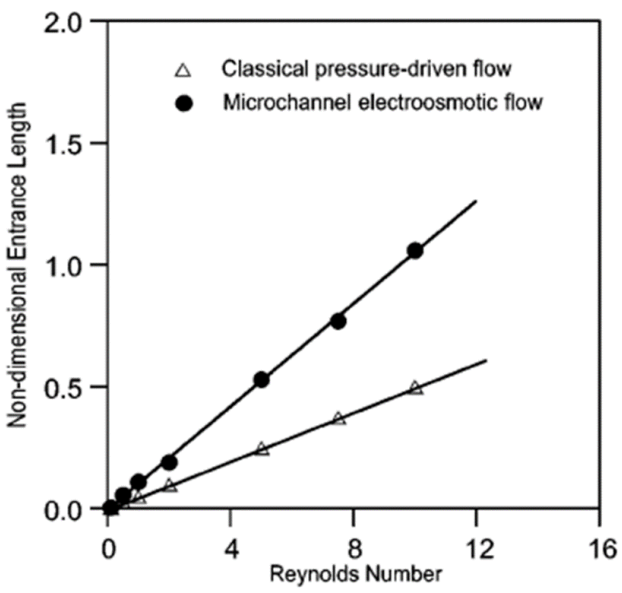

3.( ) Santiago (2001) discussed the role of inertial and pressure effects on electrokinetic flows. As shown below, his analysis divided the vicinities of an electrokinetic flow's electric double layer into two regions, namely the *inner flow region* and the *outer flow region*. The inner flow region has large charge density and high viscous stress, whereas the outer region is the space further from the wall. The two regions are separated by the so-called *slip plane*. Under certain constraints, Santiago argued, the electroosmotic flow in the outer flow region is such that its velocity field becomes simply equal to the local electric field multiplied by a constant. Specifically, similarity between velocity field and electric field in the outer flow region holds if electric double layers are thin compared to channel dimensions, the ζ-potential is uniform, fluid properties are uniform, channel walls are electrically insulating, and the product of Reynolds and Strouhal numbers is very large.

Recommended research: Santiago (2001).

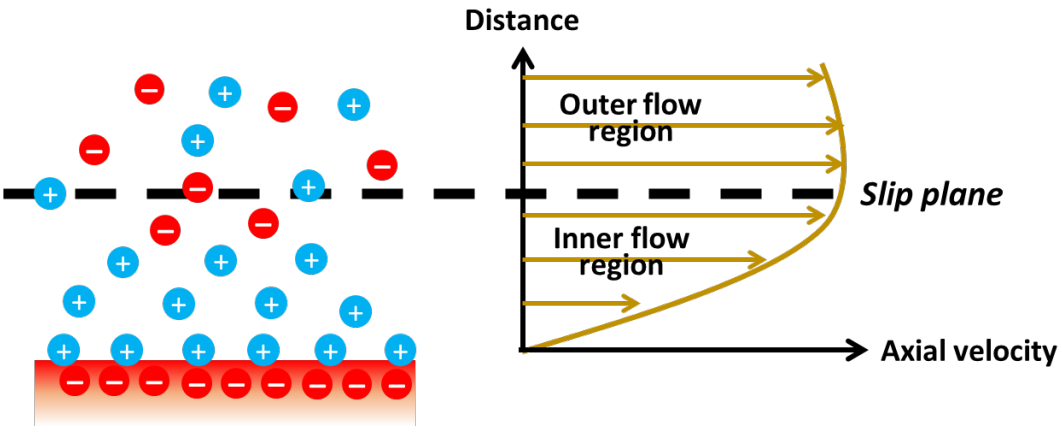

In most analyses of electroosmotic flows, the ionic distribution in the electric double layer is assumed to follow the equilibrium Boltzmann distribution, which leads to the Poisson-Boltzmann equation often used to model the electric potential induced by these ions. However, convective transport of ions may be expressive in some situations of practical interest. In these situations, the Boltzmann distribution is not valid and the Nernst-Planck equation, which affords a more exact picture of the distribution of ions in the EDL, must be used instead. Park *et al.* (2007) conducted numerical simulations to compare the performance of a model based on the PB equation and a model based on the NP equation. The simplest geometry they used was the straight two-dimensional microchannel illustrated below. Below the geometry schematic we have the longitudinal distribution of dimensionless ζ-potential, which equals 1.0 in a central segment that includes section *A*, begins to decrease at section *B*, and becomes zero at section *D*; also, at section *C* the potential $\zeta = 0.5$. Park's team ran equivalent simulations for two combinations of dimensionless parameters, one of which resulted in a thin electric double layer and the other resulted in a much thicker EDL.

4.( ) Park's team showed that at all four sections the velocity-profile predictions from the PB model were very similar to those of the NP model, regardless of the thickness of the electric double layer. ■ **(A black square indicates the end of a multi-paragraph statement.)**

Recommended research: Park *et al.* (2007).

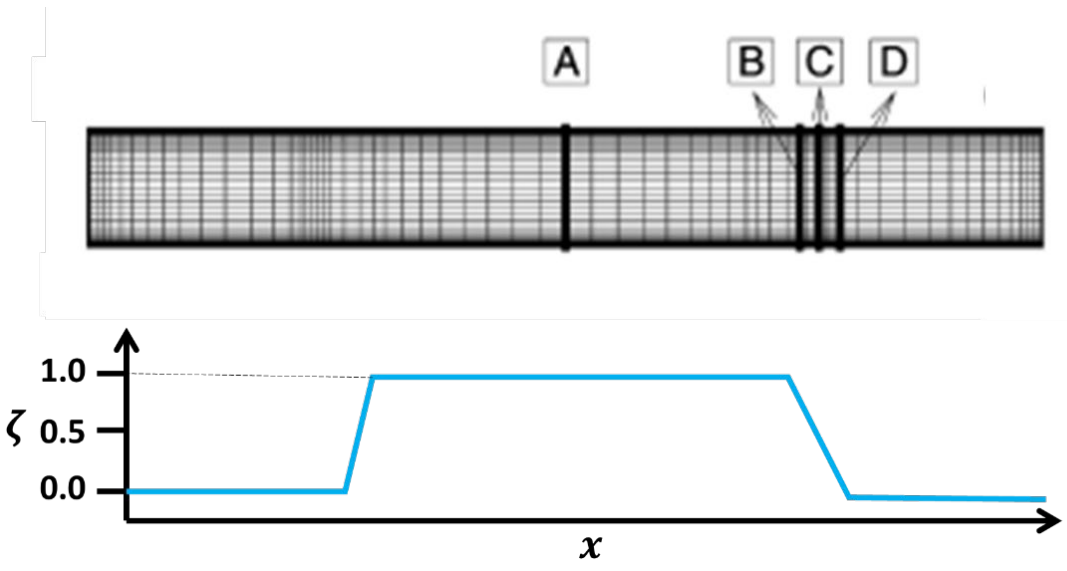

5.( ) Wang and Kang (2010) used a lattice Boltzmann algorithm to simulate electrokinetic flows in microchannels. The lattice Boltzmann approach, they noted, offers insights that would be difficult to glean from 'traditional' numerical schemes. For instance, the effect of ion valence on electroosmotic flows in microchannels is not easily ascertained, because the net charge term that appears in the electrokinetic equations is hard to linearize if the absolute value of the valence ratio $|z_1 : z_2|$ (where z_1 denotes the valence of the positive ions and z_2 denotes the valence of the negative ones) is not 1 : 1. The lattice Boltzmann approach does away with this issue because there is no need for such linearization at all. With this in mind, Wang and Kang showed that changes in ionic valence do in fact influence electric potential distribution, velocity profiles, and Debye length. Importantly, Wang and his colleague found that, contrary to commonly employed simplifications, in their algorithm the Debye length achieved for ions with 1 : 2 valence ratio did not lead to the same value obtained for ions with 2 : 1 valence ratio.

Recommended research: Wang and Kang (2010).

Patankar and Hu (1998) conducted a three-dimensional numerical study of electroosmotic flow using the SIMPLER finite-volume algorithm. Their geometry of choice was a cross-channel device such as the one illustrated below.

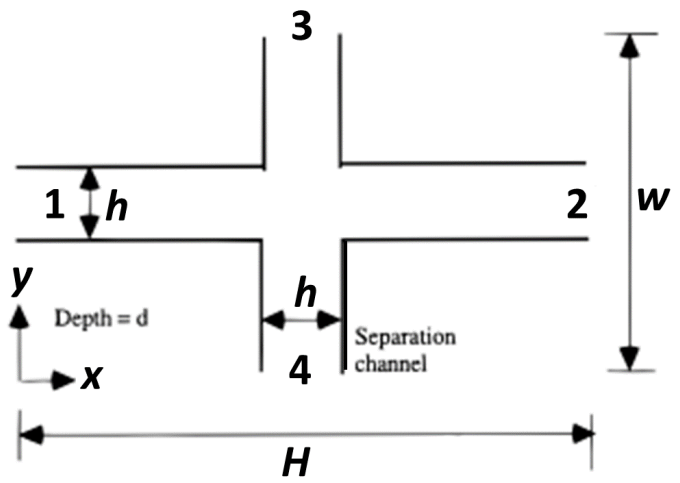

6.( ) The velocity streamlines at the intersection of the channels are shown below for different Reynolds numbers. From the spacing of the streamlines, it is clear that velocity magnitudes were found to be greatest near the walls of the channels. ■

Recommended research: Patankar and Hu (1998).

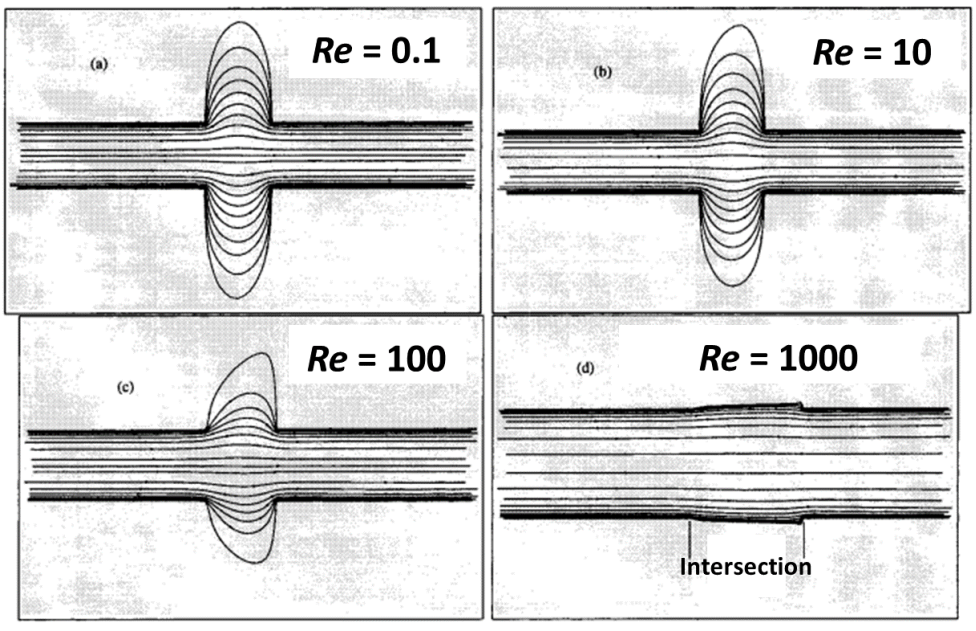

7.( ) A few years after Patankar and Hu published the results of their simulations, Ren *et al.* (2003) reported the results of their own study of electroosmotic flow in crossing microchannels. Unfortunately, Ren's discretization scheme relied on a high density of large-aspect-ratio control volumes, which made their simulations much more computationally expensive than previous efforts.

Recommended research: Ren *et al.* (2003).

Xuan and Li (2005) developed a comprehensive model for electroosmotic flow of microchannels with arbitrary geometry and arbitrary ζ-potential. In addition to its remarkable scope and generality, their model stands out for providing a simple yet effective treatment of microfluidic channels under AC fields. The AC electroosmotic velocity of a liquid in a microchannel closely follows the surrounding electric field at low frequencies, just as a DC electroosmotic velocity would. At high frequencies, however, there are substantial variations in both the phase and the amplitude of the fluid velocity over the channel cross-section. It is desirable to establish a critical frequency over which there is a visible change in either the phase or the amplitude of the electroosmotic velocity with respect to the applied electric field. In order to obtain an analytical expression for this critical frequency, Xuan and Li considered a cylindrical microchannel with a uniform wall ζ-potential. If it is assumed that a 5% change of 2π in phase occurs at the critical frequency $\Omega_{\text{crit},\phi}$, we have

$$\angle\left[\frac{I_0\left(\sqrt{in\Omega_{\text{cr},\phi}}\times r\right)}{I_0\left(\sqrt{in\Omega_{\text{cr},\phi}}\right)}\right]=-2\pi\times 0.05=-0.314\ \text{rad}$$

where $n = 1, 2, 3, \ldots$, $i=\sqrt{-1}$, r is radial distance, $\angle$ denotes angle, and I_0 is the modified Bessel function of the first kind and order zero. The negative sign is attributed to the phase lag of electroosmotic velocity relatively to the electric field. Clearly, the critical frequency is position-dependent and its minimum appears at the axis, that is, at $r = 0$. Under the base frequency, such that $n = 1$, and with $r = 0$, the equation above can be solved for $\Omega_{\text{cr},\phi}$ to yield

$$\Omega_{cr,\phi}=1.2705$$

If, instead, we define a critical frequency $\Omega_{\text{cr}.A}$ on the basis of a 5% change in amplitude, we may write

$$\left|\frac{I_0\left(\sqrt{in\Omega_{\text{cr},A}}\times r\right)}{I_0\left(\sqrt{in\Omega_{\text{cr},A}}\right)}\right|=0.95$$

8.( ) In this case, with $n = 1$ and $r = 0$, the value of $\Omega_{\text{cr},A}$ is found to be greater than 2.0. ■

Recommended research: Xuan and Li (2005).

Wang *et al.* (2007) used a lattice Poisson-Bolzmann scheme to assess the effects of surface roughness and cavitations on electroosmotic flows. Their results were interesting; for one, they found that, contrary to intuition, the maximum velocity obtained in a microchannel section increases with roughness height.

9.( ) That said, Wang and his colleague concluded that the effect of cavitations on flow rate is much more pronounced than the effect of surface roughness. ■

Recommended research: Wang *et al.* (2007).

Yang *et al.* (2011) studied the dynamics of capillary-driven liquid flow in open, hydrophilic channels embedded in a hydrophobic surface for two of the most common microchannel geometries used in microfluidic applications: rectangular and curved (see below). One of those workers' goals was to experimentally test the validity of the Washburn equation, which predicts a linear dependence between the squared position of a travelling meniscus, x^2, and time, t.

10.( ) Importantly, Yang's team found that the linear behavior associated with the Washburn equation was found to be independent of the exact shape of the cross-section, that is, irrespective of whether the channels were rectangular or curved. ■

Recommended research: Yang *et al.* (2011).

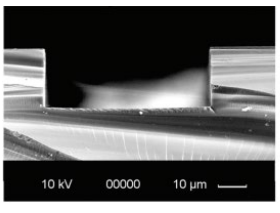

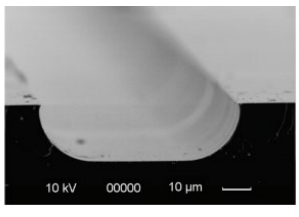

Cherlo *et al.* (2010) conducted experiments of liquid-liquid two-phase flow in a microchannel. Their two liquids of choice were water and kerosene, and the microchannel material was Perspex. Their main goals were to measure fluid slug lengths – in view of the fact that slug lengths are important in determining the performance of a two-phase flow – and establish how they could be affected by variations in flow rate, viscosity, surface tension, and other parameters.

11.( ) Cherlo's team found that viscosity significantly affected slug length; specifically, exchanging kerosene for coconut oil, which has greater viscosity, led to shorter slug lengths. On the other hand, Cherlo's FLUENT simulations indicated no significant changes in slug length when surface tension values were modified. ■

Recommended research: Cherlo *et al.* (2010).

12.( ) Ookawara *et al.* (2004) introduced a new micro-separator/classifier based on a curved channel with rectangular cross-section. The curved geometry of the microchannels was shown to generate so-called Dean vortices, which were associated with secondary velocities $V_{ave,Dean}$ described by the power law

$$V_{\text{ave,Dean}}\left[\text{m/s}\right] = 1.8\times10^{-4}\,\text{De}^{1.63}$$

where *De* is the Dean number. With reference to this equation and assuming Stokes drag to be valid, consider a 2-μm diameter spherical particle immersed in a fluid with dynamic viscosity equal to 0.001 Pa·s. The particle is engulfed in a secondary vortex with Dean number equal to 30. Given these data, we conclude that the particle is under the effect of a drag force greater than 800 pN. (1 piconewton = 10^{-12} N).

Recommended research: Ookawara *et al.* (2004).

13.( ) Flow of non-Newtonian fluids is important in microfluidic research because micro- and nanoscale devices often involve eminently nonlinear fluids such as blood and polymeric solutions. Tang *et al.* (2009) used a lattice Boltzmann numerical model to study flow of power-law fluids in microchannels. Noting that plug-like electroosmotic flow is a boon for applications such as micropumps and mixers, Tang's team maintained that, in their simulations at least, plug-like velocity profiles are easier to achieve with shear-thickening fluids than with shear-thinning ones.

Recommended research: Tang *et al.* (2009).

14.( ) Zhao and Yang (2013) developed analytical solutions for electroosmotic flow of power-law non-Newtonian fluids in cylindrical microchannels. Crucially, they found that Helmholtz-Smoluchowski velocity in such flows is distinctly dependent on the geometry of the conduit, in contrast to what is generally observed in, say, electroosmotic flows of planar surfaces and parallel plates.

Recommended research: Zhao and Yang (2013).

Zhuo *et al.* (2006) used a finite volume element (FVM) code to model convective heat transfer in microchannels of trapezoidal and triangular cross-section. With the aim of comparing numerical results with experimental data, Zhuo's team simulated the two microchannel geometries at a wide range of Reynolds numbers, namely $30 \leq Re \leq 400$.

15.( ) Interestingly, for Reynolds numbers greater than 100, Zhuo's team found that the Nusselt number *Nu* for the thermally fully-developed region of both the trapezoidal and triangular numerical schemes were shown to be linearly proportional to the corresponding *Re*. However, this relationship did not hold at lower Reynolds numbers. ■

Recommended research: Zhuo *et al.* (2006).

It is well-known that heat transfer inside flow passages can be enhanced by using passive surface modifications such as rib turbulators, protrusions, pin fins, and dimples. Previous research at the macroscale level has shown that, of these modifications, dimples may offer the best enhancement of heat transfer with the least penalty in pressure drop. With this in mind, Wei *et al.* (2007) conducted numerical simulations to assess heat transfer in a rectangular microchannel with one dimpled bottom surface. The computational domain they used is illustrated to the side; all dimensions are in μm; the arrows indicate the direction of fluid flow.

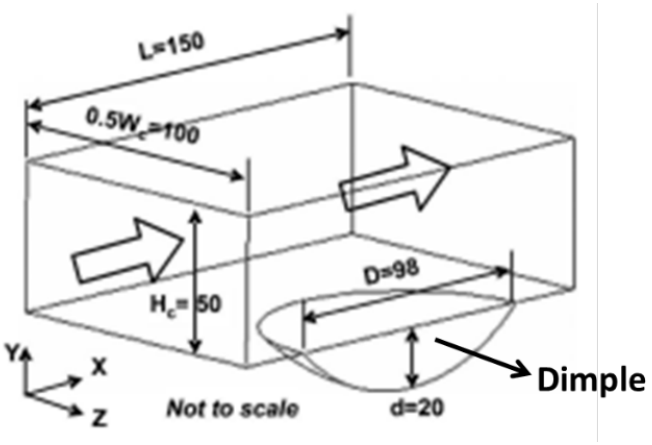

16.( ) Wei's team found that the addition of a dimple did, in fact, enhance microscale heat transfer. Crucially, they noted that heat transfer enhancement was greatest within the dimple, where a large zone of flow recirculation is present. ■

Recommended research: Wei *et al.* (2007).

17.( ) Leshansky and Pismen (2009) developed a 2D model of droplet breakup in a microfluidic T-junction. Their work relies on simple geometric arguments and agrees well with numerical simulations at low capillary numbers – and, they note, even moderate *Ca* values, too. The main shortcoming of the Leshansky-Pismen model, arguably, was the fact that it cannot be readily extended to asymmetric T-junctions (i.e., junctions where the daughter channels have different hydraulic resistances).

Recommended research: Leshansky and Pismen (2009).

Mukherjee and Kandlikar (2005) developed a numerical model to study flow of a vapor bubble inside a microchannel. The following figure shows the evolution of velocity vectors at the central vertical plane of their hypothetical microchannel. Mukherjee and his colleague went on to explore the effect of different parameters on the flow field. They found that increasing Reynolds number or inlet temperature at the channel inlet led to faster bubble growth.

18.( ) On the other hand, Mukherjee and Kandlikar noted that including gravitational effects had no effect on bubble growth rate. ■

Recommended research: Mukherjee and Kandlikar (2005).

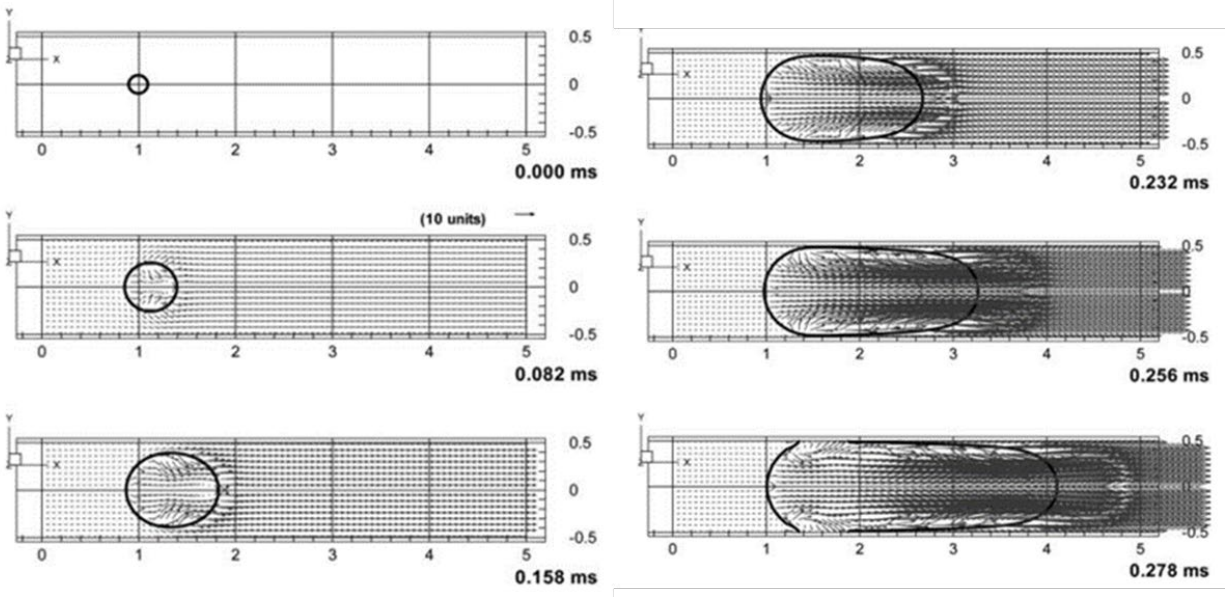

Velocity vectors at the central vertical plane of the computational domain. From Mukherjee and Kandlikar (2005). © 2005 Springer-Verlag. Reproduced with permission.

Lin *et al.* (2004) introduced a microfluidic device that can be used to generate temporal and spatial concentration gradients. Lin's team used a "mixer module" design to generate mixtures of two fluidic inputs, one for a FITC-Dextran solution and another for a buffer solution, and showed that the desired final concentration of a FITC-Dextran solution could be manipulated by adjusting the relative flow rates of each input. Further, by manipulating the two inputs while maintaining the same total flow rate, the slope, baseline and the direction of the linear concentration gradients could be changed at will.

19.( ) One limitation of the microfluidic device introduced by Lin's team is that it is restricted to linear gradients; in other words, the device is not capable of generating or controlling nonlinear spatial concentration gradients. ■

Recommended research: Lin *et al.* (2004).

20.( ) In a three-dimensional viscoelastic focusing scheme, the dimensionless critical radius of the circular microchannel to be used is 0.16, the blockage ratio is 0.11, and the Deborah number is 0.025. Accordingly, we surmise that the ratio of required channel length L_A to radius R for efficient focusing is greater than 2200. **(See the Additional Information section for details on this statement.)**

Recommended research: D'Avino *et al.* (2012).

ADDITIONAL INFORMATION

1.Electroviscous effects on pressure-driven liquid flow in microchannels (Li, 2004)

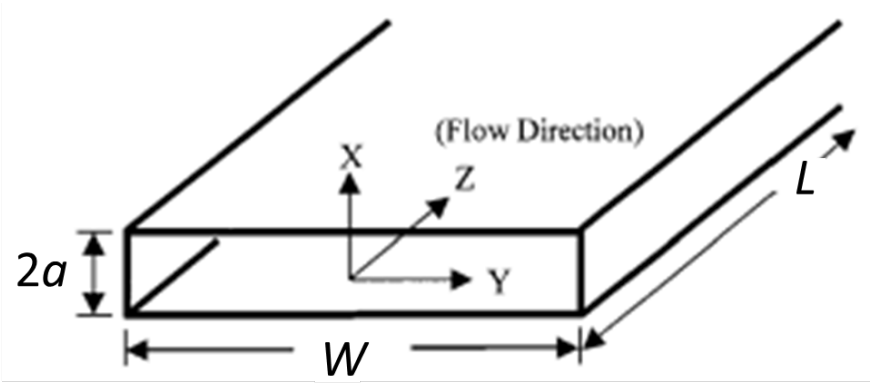

When a liquid is forced through a microchannel under an applied hydrostatic pressure, the counterions in the diffuse layer (mobile part) of the electric double layer are carried towards the downstream end, resulting in an electrical current in the pressure-driven flow direction. When ions are displaced in a liquid, they pull the liquid molecules along with them, a phenomenon that, in macroscopic terms, leads to a liquid flow in the opposite direction of the pressure-driven flow. The overall result is a reduced flow rate in the pressure-drop region. A microchannel pressure-driven flow with a retarding electrokinetic effect can be described with the dimensionless velocity profile

$$\bar{V}_z = \frac{G_1}{2}\left(1-\bar{X}^2\right) - \frac{2G_2\bar{E}_s\bar{\zeta}}{K^2}\left[1-\left|\frac{\sinh\left(K\bar{X}\right)}{\sinh\left(K\right)}\right|\right]$$

$\bar{V}_z$ is the normalized axial velocity, $\bar{X} = x/a$ is the normalized distance between plates, $\bar{E}_s = E_s/\zeta_0$ is the ratio of the applied electric field E_s to the (zeta) potential ζ_0 at the wall, and $\bar{\zeta} = (ze\zeta_0/k_BT)$ is a normalized zeta-potential where z is the ionic valence, $e \approx 1.60\times10^{-19}$ C is the elementary charge, $k_B \approx 1.38\times10^{-23}$ J/K is Boltzmann's constant, and T is temperature. Dimensionless parameter G_1 is given by

$$G_1 = \frac{a^2 P_z}{\mu V_0}$$

where:

→ a is the half-distance between plates;

→ $P_z = \Delta p/L$ is the pressure drop along the length L of the channel;

→ μ is the dynamic viscosity of the fluid;

→ V_0 is the axial velocity at the center of the channel.

Parameter G_2 is given by

$$G_2 = \frac{n_\infty zea^2\zeta_0}{\mu V_0 L}$$

where:

→ n_∞ is the bulk ion concentration;

→ z is the valence of the ions (which is assumed to be the same for positive and negative ones);

→ e is the elementary charge ≈ 1.60×10^{-19} C;
→ a is the half-distance between plates;
→ ζ_0 is the potential at the wall;
→ μ is the dynamic viscosity of the fluid;
→ V_0 is the axial velocity of the bulk fluid;
→ L is the length of the channel.

Parameter K is a scaled Debye-Hückel parameter:

$$K = a\left(\frac{2n_\infty z^2 e^2}{\varepsilon\varepsilon_0 k_b T}\right)^{1/2}$$

where:

→ a is the half-distance between plates;
→ n_∞ is the bulk ion concentration;
→ z is the valence of the ions (which is assumed to be the same for positive and negative ones);
→ e is the elementary charge ≈ 1.60×10^{-19} C;
→ ε is the permittivity of the fluid;
→ ε_0 is the vacuum permittivity ≈ 8.85×10^{-12} F m^{-1}
→ k_b is Boltzmann's constant ≈ 1.38×10^{-23} J/K;
→ T is temperature.

2.Particle focusing induced by viscoelasticity of the suspending fluid in a circular microchannel (D'Avino *et al.*, 2012)

D'Avino *et al.* (2012) showed that transversal migration of particles suspended in a viscoelastic suspension can be controlled by the rheological properties of the suspending liquid. The formula used to model a viscoelastic particle focusing scheme is

$$\frac{L_A}{R} = -\frac{A\log\left(\frac{r_A}{R-a}\right)}{\beta^2 De}$$

where A = 0.34; L_A is the 'alignment length' needed to achieve a certain focusing of particles within a region of radius r_A; R is the radius of the microtube; a is the radius of the particles; β is the blockage ratio (i.e., the ratio of particle radius to the radius of the microchannel); De is the Deborah number of the viscoelastic suspension; $r_A/(R-a)$ is also known as the dimensionless critical radius. D'Avino's paper provides practical formulas that more straightforwardly relate alignment length to flow rate and pressure drop; see their paper for details.

SOLUTIONS

P.1 ➡ *Solution*

1.False. We first compute the electric force imparted on the ion,

$$F_e = zeE = 1\times\left(1.6\times10^{-19}\right)\times12{,}000 = 1.92\times10^{-15}\ \text{N}$$

Then, appealing to Newton's second law, the acceleration a is

$$F_e = ma \rightarrow a = \frac{F_e}{m}$$

$$\therefore a = \frac{1.92\times10^{-15}}{6.5\times10^{-26}} = \boxed{2.95\times10^{10}\ \text{m/s}^2}$$

2.True. The terminal velocity of the ion equals the product of ion mobility and electric field intensity:

$$V = \mu_{EP}E = \left(5.0\times10^{-8}\right)\times12{,}000 = 6.0\times10^{-4}\ \text{m/s}$$

$$\therefore \boxed{V = 600\,\mu\text{m/s}}$$

3.False. The fluid velocity is given by the product of electroosmotic mobility and electric field intensity:

$$u = \mu_{\text{EO}} E = \left(1.6\times10^{-8}\right)\times\left(120\times10^{2}\right) = 1.92\times10^{-4}\ \text{m/s}$$
$$\therefore u = 192\ \mu\text{m/s}$$

Then, the volumetric flow rate is determined as

$$Q = uA = 192\times200 = \boxed{38,400\,\mu\text{m}^3/\text{s}}$$

4.True. We first compute the flow rate for an electroosmotic flow at 1.5 kV:

$$Q = -\frac{\varepsilon\zeta}{\mu}\frac{V}{L}A$$

$$\therefore Q = -\frac{\left[80\times\left(8.85\times10^{-12}\right)\right]\times(-0.12)}{10^{-3}}\times\frac{1500}{0.1}\times\left[\frac{\pi\times\left(8.0\times10^{-6}\right)^2}{4}\right] = 6.41\times10^{-14}\ \text{m}^3/\text{s}$$

Then, appealing to the Poiseuille equation, we solve for the pressure change Δp that would produce the same flow Q,

$$Q = -\frac{\pi R^4}{8\mu}\left(-\frac{dp}{dx}\right) = \frac{\pi R^4}{8\mu}\times\frac{(-\Delta p)}{L}$$

$$\therefore -\Delta p = \frac{8Q\mu L}{\pi R^4} = \frac{8\times\left(6.41\times10^{-14}\right)\times10^{-3}\times0.1}{\pi\times\left(4.0\times10^{-6}\right)^4} = 63.8\,\text{kPa}$$

or 63,800/101,325 = 0.63 atm. Thus, a pressure of 0.8 atm would in fact suffice to generate the same amount of flow as a voltage of 1.5 kV.

5.False. As discussed in Rapp (2017), the correction factor is actually the ratio of the section's hydraulic resistance to the normalized hydraulic resistance. The compactness factor, on the other hand, is the ratio of squared perimeter to area. The two concepts are not entirely independent, though, and can be related in interesting ways – e.g., for an elliptical cross-section, the correction factor α increases linearly as the compactness factor C is raised for a given aspect ratio r; see below.

Reference: Rapp (2017).

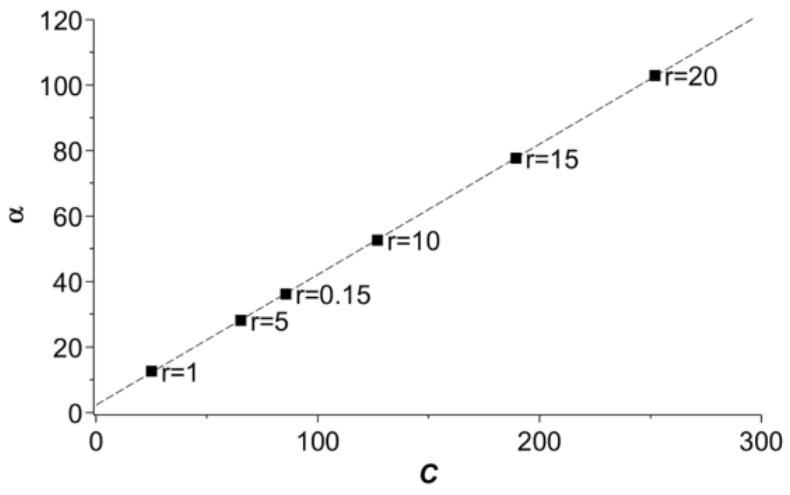

6.True. Indeed, the Poisson-Boltzmann equation in spherical coordinates has no analytical solution. One well-known means to make the P-B equation tractable is to rescale the radial coordinate r and assume that the electric potential κa is much lower than the thermal potential $k_B T/q$, so that the equation can be linearized. This approach is sometimes known as the *Debye-Hückel approximation.*

7.False. Jurin's law actually maintains that the height of capillary rise is *inversely* proportional to the radius of the tube. One simple mathematical formulation of this result is

$$h = \frac{2\gamma\cos\theta}{\rho g R}$$

where γ is surface tension, θ is the contact angle, ρ is the density of the fluid, $g \approx 9.81\ \text{m/s}^2$, and R is the radius of the tube. Clearly, $h \propto R^{-1}$.

8.True. Tanner's law relates the dynamic contact angle θ_d, the static contact angle θ_s, and the capillary number Ca,

$$\theta_d^3 - \theta_s^3 = A \times Ca$$

where A is a constant. For small capillary number, the equation may be restated as

$$\theta_d \left(\theta_s^3 + A \times Ca\right)^{1/3} \approx \theta_s \left(1 + \frac{1}{3}\frac{A \times Ca}{\theta_s^3}\right)$$

$$\therefore \theta_d - \theta_s = \frac{1}{3}\frac{A \times Ca}{\theta_s^2}$$

Hence, for small Ca the difference between contact angles is indeed linearly proportional to the capillary number.

9.False. In Taylor-Aris dispersion for cylindrical conduits, the effective diffusion D_{eff} reads

$$D_{\text{eff}} = D\left(1 + \frac{\text{Pe}^2}{48}\right)$$

Hence, the missing number is 48.

P.2 ➡ *Solution*

Part 1: The Debye length is the reciprocal of the Debye-Huckel parameter, that is,

$$\frac{1}{k} = \left(\frac{\varepsilon\varepsilon_0 k_B T}{2z^2 e^2 n_\infty}\right)^{1/2}$$

The bulk ionic number concentration n_∞ can be obtained from the product

$$n_\infty = 1000 N_a M = 1000 \times \left(6.02 \times 10^{23}\right) \times 10^{-3} = 6.02 \times 10^{23}\ \text{m}^{-3}$$

The ionic valence z = 1; all other variables are given, so that

$$\frac{1}{k} = \left[\frac{40 \times \left(8.85 \times 10^{-12}\right) \times \left(1.38 \times 10^{-23}\right) \times 298}{2 \times 1^2 \times \left(1.60 \times 10^{-19}\right)^2 \times \left(6.02 \times 10^{23}\right)}\right]^{1/2} = 6.87 \times 10^{-9}\ \text{m}$$

$$\therefore \boxed{\lambda_D = 6.87\,\text{nm}}$$

Part 2: We start off with a simple expression for reciprocal Debye length,

$$k^{-1} = \left(\frac{e^2}{\varepsilon\varepsilon_0 k_B T}\sum_{i=1}^{N} z_i^2 n_{i,\infty}\right)^{-1/2} \quad \text{(I)}$$

where the ionic concentration $n_{i,\infty}$ can be adjusted as

$$n_{i,\infty} = M_i \frac{\text{mol}}{\text{L}} \times \frac{1000\,\text{L}}{\text{m}^3} \times \frac{1}{\text{mol}} N_A$$

$$\therefore n_{i,\infty} = 1000 M_i N_A$$

so that, in equation (I),

$$k^{-1} = \left(\frac{e^2}{\varepsilon\varepsilon_0 k_B T}\sum_{i=1}^{N} z_i^2 n_{i,\infty}\right)^{-1/2} = \left(\frac{1000 N_A e^2}{\varepsilon\varepsilon_0 k_B T}\sum_{i=1}^{N} z_i^2 M_i\right)^{-1/2}$$

Taking $\varepsilon = 6.95 \times 10^{-10}$ F·m^{-1} as the permittivity of water at 298 K, we substitute above to obtain

$$k^{-1} = \left(\frac{1000 \times \left(6.02 \times 10^{23}\right) \times \left(1.60 \times 10^{-19}\right)^2}{\left(6.95 \times 10^{-10}\right) \times \left(1.38 \times 10^{-23}\right) \times 298}\sum_{i=1}^{N} z_i^2 M_i\right)^{-1/2}$$

$$\therefore k^{-1} \approx 4.306\times10^{-10}\left(\sum_{i=1}^{N} z_i^2 M_i\right)^{-1/2}$$

as we intended to show.

Part 3: The molarity of KCl upon mixing is

$$M\left[\mathrm{KCl}\right] = 0.02\times\frac{800}{800+600} = 1.14\times10^{-2}\ \mathrm{M}$$

The updated molarity of Na_2SO_4, in turn, is

$$M\left[\mathrm{Na_2SO_4}\right] = 0.0018\times\frac{600}{800+600} = 7.71\times10^{-4}\ \mathrm{M}$$

Now, we can write for KCl and K_2SO_4,

$$\sum z_i^2 M_i = \left[1^2\times\left(1.14\times10^{-2}\right)+1^2\times\left(1.14\times10^{-2}\right)\right]+$$
$$+\left[1^2\times\left(7.71\times10^{-4}\right)\times2+2^2\times\left(7.71\times10^{-4}\right)\right] = 0.0274$$

Substituting in the formula derived just now, we find that

$$k^{-1} = 4.30\times10^{-10}\times0.0274^{-1/2} = 2.60\times10^{-9}\ \mathrm{m}$$
$$\therefore \boxed{k^{-1} = 2.60\ \mathrm{nm}}$$

P.3 ➡ *Solution*

The appropriate constants are computed below.

$$G_1 = \frac{a^2 P_z}{\mu V_0} = \frac{\left(12.5\times10^{-6}\right)^2\times\left(1\times101{,}325/0.01\right)}{\left(9.0\times10^{-4}\right)\times1.0} = 1.76$$

$$G_2 = \frac{n_\infty z e a^2 \zeta_0}{\mu V_0 L} = \frac{\left(6.02\times10^{20}\right)\times1\times\left(1.60\times10^{-19}\right)\times\left(12.5\times10^{-6}\right)^2\times\left(100\times10^{-3}\right)}{\left(9.0\times10^{-4}\right)\times1.0\times0.01} = 1.67\times10^{-4}$$

$$K = a\left(\frac{2n_\infty z^2 e^2}{\varepsilon\varepsilon_0 k_b T}\right)^{1/2} = \left(12.5\times10^{-6}\right)\times\left[\frac{2\times\left(6.02\times10^{20}\right)\times1^2\times\left(1.60\times10^{-19}\right)^2}{88\times\left(8.85\times10^{-12}\right)\times\left(1.38\times10^{-23}\right)\times310}\right]^{1/2} = 38.0$$

The dimensionless velocity profile is plotted to the side. In addition, we have also plotted the profile expected for a channel flow with no electrokinetic effects, which is obtained by neglecting the second term in the velocity-profile equation, giving

$$\bar{V}_z = \frac{G_1}{2}\left(1-\bar{X}^2\right)$$

As can be seen, the velocity profile that includes electrokinetic effects is consistently less than the profile for purely pressure-driven flow.

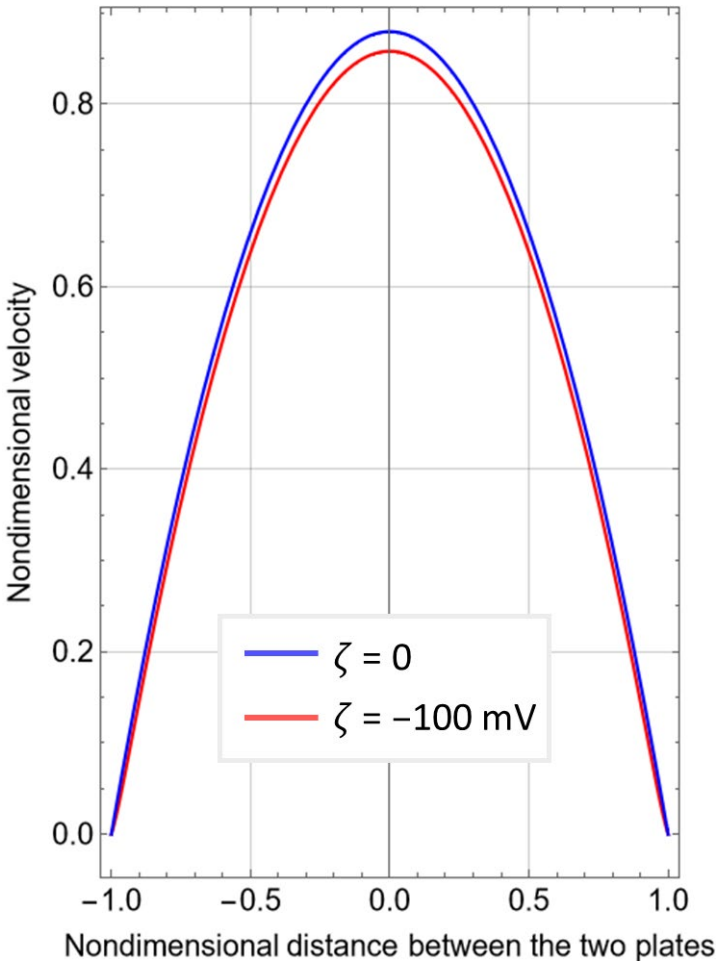

P.4 ➡ ***Solution***

We first integrate the reduced *x*-momentum equation,

$$\mu\frac{d^2u}{dy^2}=0\rightarrow u\left(y\right)=C_1y+C_2\quad\text{(I)}$$

where C_1 and C_2 are integration constants. The system is subject to two boundary conditions, the first of which is

$$u\left(y=0\right)=u_{\text{slip}}=\bar{\lambda}\left.\frac{du}{dy}\right|_{y=0}\quad\text{(II)}$$

where u_{slip} is the slip velocity at the lower wall and $\bar{\lambda}$ is the mean free path. Similarly, the second boundary condition refers to the slip velocity at the upper plate:

$$u\left(y=h\right)=U-u_{\text{slip}}=U-\bar{\lambda}\left.\frac{du}{dy}\right|_{y=0}$$

where U is the velocity with which the upper plate is being displaced. Now, from the definition of Knudsen number,

$$\text{Kn}=\frac{\bar{\lambda}}{h}\rightarrow\bar{\lambda}=h\times\text{Kn}$$

Substituting (II) in the integrated velocity profile,

$$u\left(y=0\right)=C_1\times0+C_2=u_{\text{slip}}$$

$$\therefore u_{\text{slip}}=\bar{\lambda}\left.\frac{du}{dy}\right|_{y=0}=C_2$$

Then, noting that $du/dy = C_1$ (from the first integration of (I)),

$$C_2=h\times\text{Kn}\times C_1\quad\text{(III)}$$

and

$$U-\bar{\lambda}\left.\frac{du}{dy}\right|_{y=0}=U-h\times\text{Kn}\times C_1=C_1h+C_2$$

Solving for C_1,

$$C_1=\frac{U}{h\left(1+2\text{Kn}\right)}$$

Accordingly, we may substitute C_2 into (III) to obtain

$$C_2=\cancel{h}\times\text{Kn}\times\frac{U}{\cancel{h}\left(1+2\text{Kn}\right)}=\frac{\text{Kn}\times U}{1+2\text{Kn}}$$

Lastly, we substitute C_1 and C_2 into (I) to obtain the velocity profile

$$\underline{u\left(y\right)=\frac{U}{1+2\text{Kn}}\left[\left(\frac{y}{h}\right)+\text{Kn}\right]}$$

Importantly, note that, as $Kn \rightarrow 0$,

$$u\left(y\right)\big|_{\text{Kn}\rightarrow0}=\frac{U}{1+2\times0}\left[\left(\frac{y}{h}\right)+0\right]=\frac{Uy}{h}$$

which is the velocity profile associated with simple shear (Couette) flow.

Next, let us turn to the temperature profile of the flow. We first write the governing equation

$$\kappa\frac{d^2T}{dy^2}+\mu\left(\frac{du}{dy}\right)^2=\kappa\frac{d^2T}{dy^2}+\frac{\mu}{\kappa}\left[\frac{U}{h\left(1+2\text{Kn}\right)}\right]^2=0$$

where κ is the thermal conductivity of the fluid. The equation is subject to the temperature jump condition

$$T\left(y=0\right)=T_w+T_{\text{jump}}=T_w+\frac{2\gamma}{\gamma+1}\frac{h\text{Kn}}{\text{Pr}}\left.\frac{dT}{dy}\right|_{y=0}$$

Where T_w is the temperature at the wall, γ is the specific-heat ratio and Pr is the Prandtl number. Employing symmetry, so that $\left.\frac{dT}{dy}\right|_{y=h/2}$ = 0, we integrate once to obtain

$$\frac{dT}{dy}=-Ay+C_1$$

or

$$C_1=A\frac{h}{2}$$

Integrating a second time,

$$T\left(y\right)=-\frac{A}{2}y^2+C_1y+C_2$$

Hence, at y = 0,

$$T\left(y=0\right)=-\frac{A}{2}\times0^2+C_1\times0+C_2=T_w+\frac{2\gamma}{\gamma+1}\frac{h\text{Kn}}{\text{Pr}}\left(A\frac{h}{2}\right)$$

$$\therefore C_2=T_w+\frac{2\gamma}{\gamma+1}\frac{h\text{Kn}}{\text{Pr}}\left(A\frac{h}{2}\right)$$

Finally, the temperature profile is determined to be

$$\underline{T\left(y\right)=T_w+\frac{A}{2}h^2\left[-\left(\frac{y}{h}\right)^2+\left(\frac{y}{h}\right)+\frac{2\gamma}{\gamma+1}\frac{\text{Kn}}{\text{Pr}}\right]}$$

P.5 ➡ *Solution*

Part 1: Let $1/R_{\text{approx}}$ and $1/R_{\text{exact}}$ denote the hydraulic resistances associated with the approximate and exact solutions, respectively. Dividing R_{approx} by R_{exact} brings to

$$\frac{1/R_{\text{approx}}}{1/R_{\text{exact}}}=\frac{Q_{\text{approx}}/\Delta p}{Q_{\text{exact}}/\Delta p}\approx\frac{\cancel{\frac{h^3w}{12\mu L}}\left(1-0.63\frac{h}{w}\right)}{\cancel{\frac{h^3w}{12\mu L}}\left[1-\sum_{n=1,3,5,\ldots}^{\infty}\frac{1}{n^5}\frac{192}{\pi^5}\frac{h}{w}\tanh\left(n\pi\frac{w}{2h}\right)\right]}$$

Setting $h = w$ leads to further simplification:

$$\frac{1/R_{\text{approx}}}{1/R_{\text{exact}}}=\frac{Q_{\text{approx}}/\Delta p}{Q_{\text{exact}}/\Delta p}\approx\frac{\left(1-0.63\times1\right)}{\left[1-\sum_{n=1,3,5,\ldots}^{\infty}\frac{1}{n^5}\times\frac{192}{\pi^5}\times1\tanh\left(n\pi\times\frac{1}{2}\right)\right]}$$

$$\therefore\frac{1/R_{\text{approx}}}{1/R_{\text{exact}}}=0.877$$

Thus, the approximate equation underestimates the exact one by about 12.3%.

Part 2: To obtain the improved approximation, we first note that $tanh(\pi/2)$ = 0.9172 and $tanh(3\pi/2)$ = 0.9998. Accordingly, we may retain the first term in the sum and round up the second one to 1. The ratio then becomes

$$\frac{Q_{\text{approx}}}{Q_0}=1-\sum_{n=1,3,5,\ldots}^{\infty}\frac{1}{n^5}\frac{192}{\pi^5}\tanh\left(\frac{1}{2}n\pi\right)$$

$$\therefore \frac{Q_{\text{approx}}}{Q_0} = 1 - \frac{192}{\pi^5}\tanh\left(\frac{1}{2}\pi\right) - \frac{192}{\pi^5}\sum_{n=3,5,7,\ldots}^{\infty}\frac{1}{n^5}$$

$$\therefore \frac{Q_{\text{approx}}}{Q_0} \approx 1 - \frac{192}{\pi^5}\sum_{n=1,3,5,\ldots}^{\infty}\frac{1}{n^5} + \frac{192}{\pi^5} - \frac{192}{\pi^5}\tanh\left(\frac{\pi}{2}\right)$$

$$\therefore \frac{Q_{\text{approx}}}{Q_0} \approx 1 - 0.630 + 0.627 - 0.575$$

$$\therefore \frac{Q_{\text{approx}}}{Q_0} \approx 0.422$$

The exact solution, taking the first six terms in the summation, is 0.4217, as shown in the following Mathematica code.

```
In[55]:= 1 - Sum[1/n^5 * 192/Pi^5 * Tanh[n * Pi / 2], {n, {1, 3, 5, 7, 9, 11.}}]

Out[55]= 0.421735
```

Accordingly, the improved approximation deviates from the exact solution by less than 0.1%.

P.6 ➡ *Solution*

In the case of a channel housing an interface with equal contact angles $\theta_1 = \theta_2 = \theta$, the curvature in the wide transverse direction of the flat channel is of the order $2/w$, where w is the width of the channel. Hence, inclusion of the radii of curvature in both directions leads to a Young-Laplace-like pressure drop Δp given by

$$\Delta p = \gamma\left(\frac{2}{h} + \frac{2}{w}\right)\cos\theta = \frac{2\gamma}{h}\left(1 + \frac{h}{w}\right)\cos\theta \approx \frac{2\gamma\cos\theta}{h}$$

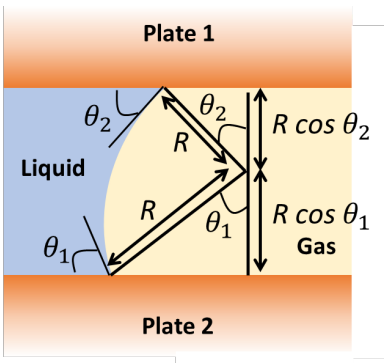

where we have used the approximation $h \gg w$, in which h is the height of the channel. Suppose now that the angles θ_1 and θ_2 at the bottom and top plates were different, as illustrated to the side. In such a case, the geometry of the figure indicates that $h = R \times \cos(\theta_1) + R \times \cos(\theta_2)$. Assuming that the only nonzero radius of curvature R is perpendicular to the plates, the pressure drop predicted by Young-Laplace theory is

$$\Delta p_{\text{surf}} = \frac{\gamma}{R} = \frac{\gamma}{h}\left[\cos(\theta_1) + \cos(\theta_2)\right] = \boxed{\frac{2\gamma}{h}\left[\frac{\cos(\theta_1) + \cos(\theta_2)}{2}\right]}$$

P.7 ➡ *Solution*

From Hagen-Poiseuille flow for channels, the flow rate is given by

$$Q = \frac{\Delta p}{L}\frac{h^2}{12\mu}A$$

However, from the Young-Laplace equation, the pressure drop is related to the wetting angle by the simple expression

$$\Delta p = \frac{2\gamma\cos\theta}{h}$$

The velocity of the meniscus is given by

$$v = \frac{dL}{dt} = \frac{Q}{hw} = \frac{\Delta p}{L}\frac{h^2}{12\mu}$$

Separating variables,

$$\frac{dL}{dt} = \frac{\Delta p}{L}\frac{h^2}{12\mu} \rightarrow LdL = \frac{\Delta p}{L}\frac{h^2}{12\mu}dt$$

Integrating,

$$\int L dL = \int \frac{\Delta p h^2}{12\mu} dt \rightarrow \frac{L^2}{2} + C = \frac{\Delta p h^2}{12\mu} t$$

where C is an integration constant, which, using $L(t = 0) = 0$, can be shown to equal zero. Then, replacing Δp with the Young-Laplace equation,

$$\frac{L^2}{2} = \frac{h^2}{12\mu} \times \frac{2\gamma \cos(\theta)}{h} \times t$$

$$\therefore \frac{L(t)}{h} = \sqrt{\frac{t}{\frac{3\mu h}{\gamma \cos(\theta)}}}$$

Denoting the denominator inside the square root as τ, we ultimately obtain

$$\underline{\frac{L(t)}{h} = \left(\frac{t}{\tau}\right)^{\frac{1}{2}}}$$

Accordingly, the meniscus advances with the square root of time. Further, the advancing meniscus speed is obtained by differentiating the result above with respect to t,

$$v = \frac{dL(t)}{dt} = \underline{\frac{h}{2\sqrt{\tau}} t^{-1/2}}$$

Accordingly, the velocity of the meniscus decreases with the square root of time.

P.6 ➡ *Solution*

1.False. This is a simple observational exercise. Upon drawing a vertical segment from $Re = 3.0$ in the horizontal axis and then tracing it to the vertical axis, we see that the effective pressure gradient needed to sustain the flow is no greater than 8 MPa/m.

2.True. Much like the previous statement, this one involves a simple observational exercise. Yang *et al.* (2001) state that the entry length of a classical fluid-dynamic flow is about $L \approx 0.06Re$, whereas for an electroosmotic flow the entry length is approximately $L \approx 0.11Re$. The difference may be ascribed to the fact that, in addition to viscous drag, electroosmotic flows must also overcome the forces elicited by electrical attraction between the fluid and the electric double layer on the channel wall; in hydrodynamic terms, this additional retarding effect implies a greater length for the transition from undeveloped to fully-developed flow.

Reference: Yang *et al.* (2001).

3.False. Santiago (2001) actually argued that similarity between velocity and electric fields hinges on *low* Reynolds numbers and *low* products of Reynolds and Strouhal numbers. Other constraints include electric double layers thin compared to channel dimension; uniform ζ-potential; uniform fluid properties; electrically insulating channel walls; parallel flow at inlets and outlets; and equal pressure at all inlets and outlets.

Reference: Santiago (2001).

4.False. Park's team found little difference in velocity profiles across sections when the electric double layer was made thin, so that ions followed the Boltzmann distribution closely. However, for thicker EDL settings, there were appreciable discrepancies between the PB- and NP-based solutions, especially at the sections with inhomogeneous ζ-potential (i.e., B, C, and D). Those workers found that in these regions the axial velocities predicted by the NP model tended to lag those extracted from the PB model. Park's team went on to compare the velocity profiles achieved in an *irregular* channel, and again the discrepancies between the PB and NP models were found to be much more pronounced for thick-EDL conditions than for thin-EDL conditions.

Reference: Park *et al.* (2007).

5.True. There are other interesting findings in that paper. For one, Wang and Kang (2010) challenged the notion, common in earlier literature, that the Poisson-Boltzmann approach breaks down for thick electric double

layers; while the disagreement between the PB model and the Nernst-Planck-based model (which they labeled the 'dynamic model') did increase as the Debye length was made thicker, the deviation was much less than suggested by previous research. For example, velocity profiles obtained with the PB approach were still accurate even when the Debye length was made 10 times thicker than the channel height.

Reference: Wang and Kang (2010).

6.False. Patankar and Hu (1998) note that the relative spacing between the streamlines (or the path lines) are in no way related to the magnitude of the velocity at a given location. In actuality, the greater density of streamlines near the walls is merely attributable to the fact that the numerical grid was made finer near those regions in order to capture close-to-wall effects.

Reference: Patankar and Hu (1998).

7.False. Ren *et al.* (2003) used square control volumes (or elements) and artificial boundaries, with the intent of saving computational time. Thus, if anything, the Ren *et al.* (2003) study stands out for its *lower* computational burden.

Reference: Ren *et al.* (2003).

8.False. The value of $\Omega_{\mathrm{cr},A}$ is obtained by solving the nonlinear equation

$$\left|\frac{I_0\left(\sqrt{i\times 1\times \Omega_{\mathrm{cr},A}}\times 0\right)}{I_0\left(\sqrt{i\times 1\times \Omega_{\mathrm{cr},A}}\right)}\right| = 0.95$$

$$\therefore \left|\frac{I_0(0)}{I_0\left(\sqrt{i\Omega_{\mathrm{cr},A}}\right)}\right| = 0.95$$

$$\therefore \left|\frac{1}{I_0\left(\sqrt{i\Omega_{\mathrm{cr},A}}\right)}\right| = 0.95$$

One easy way to solve this equation numerically is by means of Mathematica's *FindRoot* command:

```
FindRoot[Abs[BesselI[0, 0] / BesselI[0, √(I * 1.0 * Ω)]] - 0.95, {Ω, 1.0}]

{Ω → 1.85516}
```

That is, $\Omega_{\mathrm{cr},A} \approx 1.855$.

9.False. The following plots show the flow rates obtained for rough (Q_{rough}) and cavitation-laden ($Q_{\mathrm{cavitation}}$) surfaces, both of which have been normalized with the corresponding flow under smooth conditions. The horizontal axis refers to the relative geometry of the roughness and cavitations. As can be seen, a certain *D*/*w* ratio for a roughness element leads to a much lower flow rate ratio than an equivalent geometry for cavitation elements, indicating that roughness has a greater impact on microchannel electroosmotic flow than cavitation.

Reference: Wang *et al.* (2007).

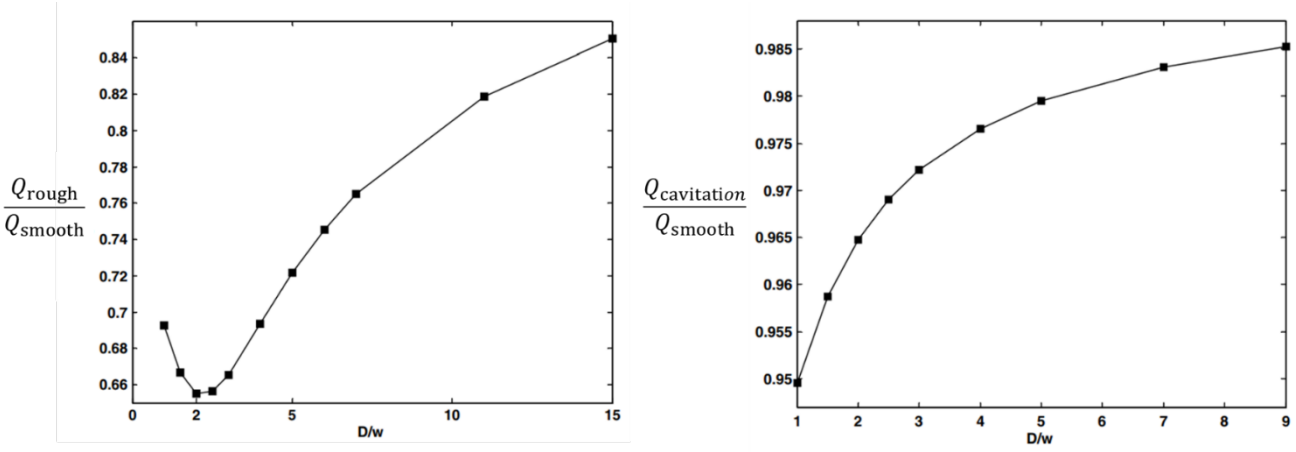

Flow rate variation with roughness (left) and cavitations (right) for a given geometry D/w. From Wang et al. *(2007). © 2007 Elsevier. Reproduced with permission.*

10.True. The final part of the statement is taken verbatim from the results section of Yang *et al.* (2011). After a brief 'accommodation' period ranging from 2 to 10 ms, Yang's team noted, a regime of linear dependence of x^2 with t appears to be well-established regardless of the shape of the cross-

section. The shape of the channel only appears in a prefactor that determines the flow rate.

Reference: Yang *et al.* (2011).

11.True. Indeed, Cherlo *et al.* (2010), upon running FLUENT simulations for a kerosene-water system with surface tension ranging from 5 to 120 mN/m, verified no significant change in slug length. However, those workers went on to report that experiments did indicate a significant dependence of slug length on surface tension. The reason for the discrepancy between computational and experimental findings, they argued, is the fact that the former allowed them to modify surface tension without changing any other thermomechanical variables, whereas in experimental settings changes in surface tension were accompanied by indirect variations in other properties, especially viscosity, that may affect the slug lengths substantially.

Reference: Cherlo *et al.* (2010).

12.True. Substituting *De* = 30 into the correlation, we get

$$V_{\text{ave,Dean}}\left[\text{m/s}\right] = 1.8\times10^{-4}\times30^{1.63} = 0.0460\,\text{m/s}$$

Then, the Stokes drag is given by

$$F_D = 3\pi\mu V_{\text{ave,Dean}}a = 3\pi\times0.001\times0.0460\times\left(2.0\times10^{-6}\right) = 8.67\times10^{-10}\ \text{N}$$

$$\therefore \boxed{F_D = 867\,\text{pN}}$$

Reference: Ookawara *et al.* (2004).

13.False. Tang *et al.* (2009) actually reported the opposite. Their previous work had shown that Newtonian flow becomes plug-like when the ratio of the channel height to Debye length becomes lower than about 10. In their simulations, using a Debye length fixed at 29.15 nm, a Newtonian fluid was shown to exhibit plug-like velocity profiles for a channel height of 0.4 μm, but not for 0.1 or 0.2 μm. In contrast, a n = 1.5 shear-thickening fluid at the same Debye length did not become plug-like for channel heights as large as 1.0 μm. A n = 0.5 shear-thinning fluid, on the other hand, displayed a plug-like profile for heights as little as 0.05 μm.

Reference: Tang *et al.* (2009).

14.True. Zhao and Yang (2013) indeed found that the HS velocity of electroosmotic non-Newtonian flow, be it shear-thickening or shear-thinning, is closely related to the factor κR, where κ is the Debye-Hückel parameter and R is the radius of the conduit.

Reference: Zhao and Yang (2013).

15.False. Zhuo *et al.* (2006) actually reported the opposite; that is, a linear relationship between Nusselt number and Reynolds numbers was verified for *Re less than* 100, and the relationship gradually broke down for *Re* > 100. This is shown below for the trapezoidal channel; the squares and circles refer to experimental and numerical data, respectively.

Reference: Zhuo *et al.* (2006).

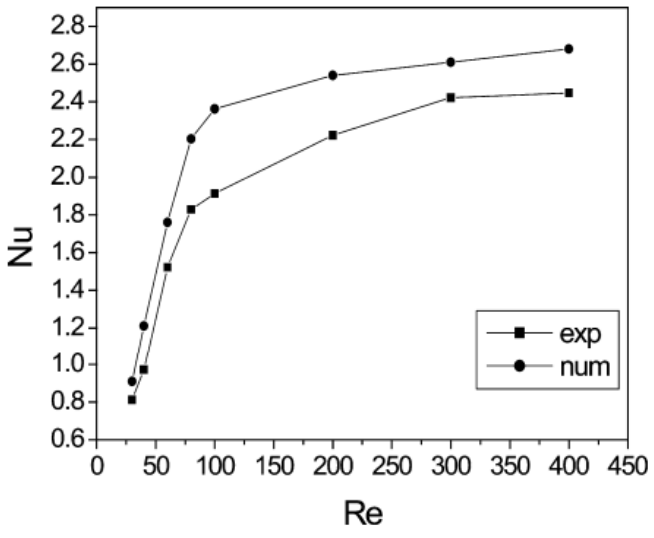

From Zhuo et al. *(2006). © 2006 Elsevier. Reproduced with permission.*

16.False. Wei *et al.* (2007) actually found that, of all regions of their computational domain, heat transfer enhancement was *weakest* within the dimple, as a result of the intense recirculation observed in that region. The larger heat transfer enhancements were found near the downstream edge of

the dimple and can be ascribed to the shear-layer reattachment, in addition to the extra advection induced by the secondary flow associated with the vortices that are shed from the dimples.

Reference: Wei *et al.* (2007).

17.True. Leshansky and Pismen (2009) indeed note that their study cannot be straightforwardly extended to asymmetric T-junctions, because in such cases the breakup process (which leads to the formation of two unequal drops) is inherently dynamic, being dominated by the mean flow direction.

Reference: Leshansky and Pismen (2009).

18.True. The following graph shows the temporal evolution of bubble equivalent diameter obtained by Mukherjee and Kandlikar (2005) with and without inclusion of gravitational effects. As can be seen, the two lines are linearly identical; earlier experiments by Kandlikar and Balasubramanian (2004) had noted similar findings.

References: Mukherjee and Kandlikar (2005); Kandlikar and Balasubramanian (2004).

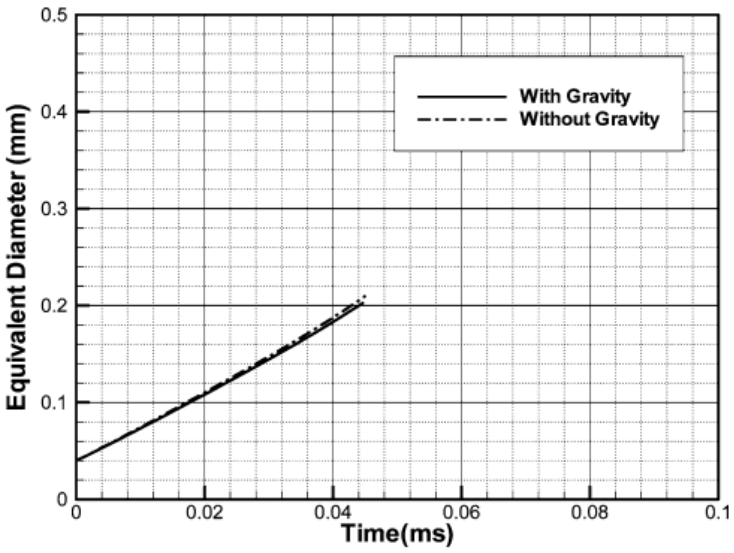

From Mukherjee and Kandlikar (2005). © 2005 Springer-Verlag. Reproduced with permission.

19.False. Much to the contrary, Lin's team showed that their device can be used to create and control spatial concentration gradients of various shapes. Indeed, they found that the device reliably produced gradient profiles of the power-law form $c(x) = ax^b$, where c is the normalized FITC-Dextran concentration as a function of the position (x) in the observation channel, and a and b are fitting parameters; the power b was found to vary from ~0.5 to ~2, and hence includes appreciably nonlinear concentration patterns. Adjustments to the configuration of the microfluidic device could be used to achieve powers b as large as ~4.2.

Reference: Lin *et al.* (2004).

20.False. The equation to use is

$$\frac{L_A}{R} = -\frac{A\log\left(\frac{r_A}{R-a}\right)}{\beta^2 De}$$

$$\therefore \frac{L_A}{R} = -\frac{0.34\times\log(0.16)}{0.11^2\times 0.025} = \underline{2060}$$

Reference: D'Avino *et al.* (2012).

REFERENCES

- BRUUS, H. (2008). *Theoretical Microfluidics*. Oxford: Oxford University Press.
- Cherlo, S.K.R., Kariveti, S. and Pushpavanam, S. (2010). Experimental and numerical investigations of two-phase (liquid-liquid) flow behavior in rectangular microchannels. *Ind Eng Chem Res*, 49(2), 893 – 899.
- D'Avino, G., Romeo, G., Villone, M.M. *et al.* (2012). Single line particle focusing induced by viscoelasticity of the suspending liquid: theory, experiments and simulations to design a micropipe flow-focuser. *Lab Chip*, 12, 1638.
- Kandlikar, S.G. and Balasubramanian, P. (2004). Effect of gravitational orientation on flow boiling of water in 1054×197 μm parallel minichannels. *In: Proceedings of the 2nd international conference on microchannels and minichannels.* New York: American Society of Mechanical Engineers.

- KLEINSTREUER, C. (2014). *Microfluidics and Nanofluidics: Theory and Selected Applications*. Hoboken: John Wiley and Sons.
- Leshansky. A.M. and Pismen, L.M. (2009). Breakup of drops in a microfluidic T junction. *Phys Fluids*, 21, 023303.
- LI, D.Q. (2004). *Electrokinetics in Microfluidics*. Amsterdam: Elsevier.
- LI, D.Q. (Ed.) (2015). *Encyclopedia of Microfluidics and Nanofluidics*. 2nd edition. Berlin/Heidelberg: Springer.
- Lin, F., Saadi, W., Rhee, S.W. *et al.* (2004). Generation of dynamic temporal and spatial concentration gradients using microfluidics devices. *Lab Chip*, 4(3), 164 – 167.
- Mukherjee, A. and Kandlikar, S.G. (2005). Numerical simulation of growth of a vapor bubble during flow boiling of water in a microchannel. *Microfluid Nanofluid*, 1, 137 – 145.
- Ookawara, S., Higashi, R., Street, D. *et al.* (2004). Feasibility study on concentration of slurry and classification of contained particles by microchannel. *Chem Eng J*, 101(1 – 3), 171 – 178.
- Park, H.M., Lee, J.S. and Kim, T.W. (2007). Comparison of the Nernst-Planck model and the Poisson-Boltzmann model for electroosmotic flows in microchannels. *J Colloid Interface Sci*, 315(2), 731 – 739.
- Patankar, N.A. and Hu, H.H. (1998). Numerical simulation of electroosmotic flow. *Anal Chem*, 70(9), 1870 – 1881.
- RAPP, B.E. (2017). *Microfluidics: Modelling, Mechanics and Mathematics*. Amsterdam: Elsevier.
- Ren, L.Q., Sinton, D. and Li, D.Q. (2003). Numerical simulation of microfluidic injection processes in crossing microchannels. *J Micromech Microeng*, 13, 739 – 747.
- Santiago, J.G. (2001). Electroosmotic flow in microchannels with finite inertial and pressure forces. *Anal Chem*, 73(10), 2353 – 2365.
- Tang, G.H., Li, X.F., He, Y.L. *et al.* (2009). Electroosmotic flow of non-Newtonian fluid in microchannels. *J Non-Newtonian Fluid Mech*, 157(1 – 2), 133 – 137.
- TIAN, W.-C. and FINEHOUT, E. (Eds.) (2008). *Microfluidics for Biological Applications*. Berlin/Heidelberg: Springer.
- Wang, M. and Kang, Q. (2010). Modelling electrokinetic flows in microchannels using coupled lattice Boltzmann methods. *J Comput Phys*, 229(3), 728 – 744.
- Wang, M., Wang, J. and Chen, S. (2007). Roughness and cavitations effects on electro-osmotic flows in rough microchannels using the lattice Poisson-Boltzmann methods. *J Comput Phys*, 226(1), 836 – 851.
- Wei, X.J., Joshi, Y.K. and Ligrani, P.M. (2007). Numerical simulation of laminar flow and heat transfer inside a microchannel with one dimpled surface. *J Electron Packag*, 129(1), 63 – 70.
- Xuan, X.C. and Li, D.Q. (2005). Electroosmotic flow in microchannels with arbitrary geometry and arbitrary distribution of wall charge. *J Colloid Interface Sci*, 289(1), 291 – 303.
- Yang, D., Krasowska, M., Priest, C. *et al.* (2011). Dynamics of capillary-driven flow in open microchannels. *J Phys Chem C*, 115(38), 18761 – 18769.
- Yang, R.-J., Fu, L.-M. and Hwang, C.-C. (2001). Electroosmotic entry flow in a microchannel. *J Colloid Interface Sci*, 244(1), 173 – 179.
- Zhao, C. and Yang, C. (2013). Electroosmotic flows of non-Newtonian power-law fluids in a cylindrical microchannel. *Electrophoresis*, 34(5), 662 – 667.
- Zhuo, L., Tao, W.-Q., He, Y.-L. (2006). A numerical study of laminar convective heat transfer in microchannel with non-circular cross-section. *Int J Therm Sci*, 45(12), 1140 – 1148.